Supporting Information for:

MORPHOLOGICAL EXPRESSION OF THE COHERENCE AND RELATIVE PHASE OF OPTICAL INPUTS TO THE PHOTOELECTRODEPOSITION OF NANOPATTERNED SE-TE FILMS

AZHAR I. CARIM[1], NICOLAS A. BATARA[2], ANJALI PREMKUMAR[2], RICHARD MAY[1], HARRY A. ATWATER[2,3] AND NATHAN S. LEWIS[1,3,4*]

[1]Division of Chemistry and Chemical Engineering

[2]Division of Engineering and Applied Sciences

[3]Kavli Nanoscience Institute

[4]Beckman Institute

California Institute of Technology

Pasadena, CA 91125

*Corresponding Author: nslewis@caltech.edu

S1. Contents

This document contains a description of the experimental and modeling/simulation methods utilized in this work (Sections S2 and S3), cross-sectional scanning-electron micrographs (Section S4), analyses of the elemental composition and the structure of the photoelectrodeposits (Sections S5 and S6), and a list of associated references (Section S7).

S2. Experimental Methods

Materials and Chemicals $(CH_3)_2CO$ (ACS Grade, BDH), H_2SO_4 (ACS Reagent, J. T. Baker), HF (49 %, Semiconductor Grade, Puritan Products), In (99.999 %, Alfa Aesar), Ga (99.999 %, Alfa Aesar), SeO_2 (99.4 %, Alfa Aesar), and TeO_2 (99+ %, Sigma-Aldrich) were used as received. H_2O with a resistivity ≥ 18.2 MΩ cm (Barnstead Nanopure System) was used throughout. n^+-Si(111) (0.004 – 0.006 Ω cm, As-doped, 400 ± 15 μm, single-side polished, Addison Engineering) was used as a substrate for deposition. Flash-Dry Silver Paint (SPI Supplies), Double/Bubble Epoxy (Hardman) and nitrocellulose-based nail polish were used to assemble the Si working electrodes.

Electrode Preparation One end of a Sn-coated Cu wire (22 AWG) was bent to form a small, flat coil and the wire was then threaded through glass tubing (6 mm O. D.) such that the coil was just outside the tubing. Epoxy was applied to seal the end of the tube from which the coil protruded. Square Si wafer sections (ca. 5 mm by 5 mm) were cut and a eutectic mixture of Ga and In was scratched into the unpolished surfaces with a carbide-tipped scribe. The wire coil was then contacted to the unpolished surface and affixed with Ag paint. Nail polish was applied to insulate the unpolished face, the wire-coil contact, and the exposed wire between the coil and epoxy seal. Immediately before deposition, the Si surface of each electrode was cleaned with $(CH_3)_2CO$, and then the Si section of the electrode was immersed in a 49 wt. % solution of HF(aq) for ~ 10 s to remove any surficial SiO_x from the Si. The electrode was then rinsed with H_2O and dried under a stream of N_2(g).

Electrode Illumination Illumination for the photoelectrochemical depositions was provided by narrowband diode (LED) sources with an intensity-weighted λ_{avg} value of 630 nm and a spectral bandwidth (FWHM) of 18 nm (Thorlabs M625L2 and M625L3). The output of each diode source

was collected and collimated with an aspheric condenser lens (Ø30 mm, f = 26.5 mm). For experiments involving simultaneous illumination with two LED sources, a polka dot beam splitter (Thorlabs BPD508-G) was utilized to combine the outputs. Both sources were incident upon the beam splitter at an angle of 45 ° from the surface normal, and thus generated coaxial output. A dichroic film polarizer (Thorlabs LPVISE2X2 or LPNIRE200-B) was placed between each source and the beam splitter to enable independent control of the polarization of each source. A 1500 grit ground-glass (N-BK7) diffuser was placed immediately in front of the photoelectrochemical cell to ensure spatial homogeneity of the illumination.

Additionally, a HeNe laser (Aerotech LSR5P) emitting at 632.8 nm in a TEM_{00} mode with linear polarization was also used an illumination source. The HeNe laser was fitted with a 10x beam expander (Melles-Griot) to create a spot that overfilled the working electrode. The output from the HeNe laser was directed at normal incidence through a zero-order λ/4 plate (Thorlabs WPQ10E-633). The λ/4 plate was rotated about the optical axis such that the fast axis of the plate was oriented at angles between 0 and 45° clockwise from the polarization axis of the laser. The presence of the λ/4 plate generated a $\phi = 90°$ phase angle between the orthogonal components of the laser illumination and provided for the generation of defined elliptical polarizations.

The light intensity incident on the electrode was measured by placing a calibrated Si photodiode (Thorlabs FDS100) instead of an electrode assembly in the photoelectrochemical cell with electrolyte, and the steady-state current response of that Si photodiode was measured. All depositions were performed with an intensity of 13.7 mW cm^{-2} at the electrode.

Photoelectrochemical Deposition Photoelectrochemical deposition was performed using a Bio-Logic SP-200 potentiostat. Deposition was performed in a single-compartment glass cell with a pyrex window. A three-electrode configuration was utilized with a graphite-rod counter electrode

(99.999 %, Sigma-Aldrich) and a Ag/AgCl reference electrode (3 M KCl, Bioanalytical Systems). Films were deposited from an aqueous solution of 0.0200 M SeO_2, 0.0100 M TeO_2, and 2.00 M H_2SO_4. Deposition was effected by biasing the n^+-Si electrode, illuminated as detailed under the above subheading (*Electrode Illumination*), potentiostatically at -0.40 V vs. Ag/AgCl for 5.00 min at room temperature. After deposition, the electrode was immediately removed from the cell, rinsed with H_2O, and then dried under a stream of N_2(g). The Si substrate with top-facing Se-Te film was mechanically separated from the rest of the electrode assembly. The nitrocellulose-based insulation and the majority of the Ag paint and In-Ga eutectic were then removed mechanically.

Microscopy Scanning electron micrographs (SEMs) were obtained with a FEI Nova NanoSEM 450 at an accelerating voltage of 5.00 kV with a working distance of 5 mm and an in-lens secondary electron detector. Micrographs obtained for quantitative analysis were acquired with a resolution of 172 pixels μm^{-1} over ca. 120 μm^2 areas. Micrographs utilized to produce display figures were acquired with a resolution of 344 pixels μm^{-1} over ca. 8 μm^2 areas.

Energy-dispersive X-ray Spectroscopy Energy dispersive X-ray spectroscopy (EDS) was performed in a Zeiss 1550VP SEM with an accelerating voltage of 15.00 kV and a working distance of 12 mm. An Oxford Instruments X-Max silicon drift detector was utilized. Spectra were collected in the range of 0 to 10 keV, and quantitative film compositions were derived from these spectra using the "INCA" software package (Oxford Instruments).

Raman Spectroscopy Raman spectra were collected with a Renishaw inVia Raman microprobe equipped with a Leica DM 2500 M microscope, a Leica N Plan 50x objective (numerical aperture = 0.75), a 1800 lines mm^{-1} grating, and a CCD detector configured in a 180° backscatter geometry. A 532 nm diode-pumped solid-state (DPSS) laser (Renishaw RL532C50) was used as the excitation source and a 10 μW radiant flux was incident on the surface

of the sample. A line focus lens was utilized to transform the circular incident beam in one dimension to generate a ca. 50 μm line at the sample. A λ/4 plate was used to circularly polarize the incident excitation. No polarizing collection optic was used.

S3. Modeling and Simulation Methods

Simulation of Film Morphology The growths of the photoelectrochemically deposited films were simulated with an iterative growth model wherein electromagnetic simulations were first used to calculate the local photocarrier-generation rates at the film surface. Then, mass addition was simulated via a Monte Carlo method wherein the local photocarrier-generation rate weighted the local rate of mass addition along the film surface.

Growth simulations began with a bare, semi-infinite planar Si substrate. In the first step, the light-absorption profile under a linearly polarized, plane-wave illumination source was calculated using full-wave finite-difference time-domain (FDTD) simulations with periodic boundary conditions along the substrate interface. In the second step, a Monte Carlo simulation was performed in which an amount of mass, equaling that of a 15 nm planar layer covering the simulation area, was added to the upper surface of the structure with a probability *F*:

$$F(G) = \left[1 + G(\mathrm{n}_0\tau_p + \mathrm{p}_0\tau_n) + G^2\frac{\tau_p\tau_n}{\mathrm{n}_i^2}\right]\prod_{i=1}^{3}\frac{x_i}{r_i} \quad \textbf{(Equation 1)}$$

where *G* is the spatially dependent photocarrier-generation rate at the deposit/solution interface, n_i is the intrinsic carrier concentration, n_0 is the electron concentration, p_0 is the hole concentration, τ_n is the electron lifetime, τ_p is the hole lifetime, x_i is the fraction of i^{th} nearest neighbors occupied in the cubic lattice, and r_i is the distance to the i^{th} nearest neighbor. The multiplicative sum in the definition of this probability (Equation 1) serves to reduce the surface roughness of the film so as to mimic the experimentally observed surface roughness.

After the initial Monte Carlo simulation, the absorbance of the new, structured film was then calculated in the same manner as for the initial planar film, and an additional Monte Carlo simulation of mass addition was performed. This process of absorbance calculation and mass

addition was repeated for a total of 20 iterations.

General Parameters Se–Te films were assumed to be undoped (i.e. $n_0 = p_0 = n_i$) and a value of $n_i = 10^{10}$ cm^{-3} was used for the intrinsic carrier concentration.[1] A value of 1 μs was used for both the electron and hole lifetimes.[2] Previously measured values of the complex index of refraction for Se-Te were utilized.[3] A value of n = 1.33 was used as the refractive index of the electrolyte, regardless of wavelength.[4] Illumination intensities identical to those used experimentally (see Section S2) were used in the simulations. Simulations of the film morphology utilized the peak intensity wavelength of the experimental sources described in Section S2. The electric field vector of the illumination was oriented parallel to the substrate. A two-dimensional square mesh with a lattice constant of 1 nm was used for the simulations. All FDTD simulations were performed using the "FDTD Solutions" software package (Lumerical).

S4. Cross-Sectional Scanning-Electron Micrographs

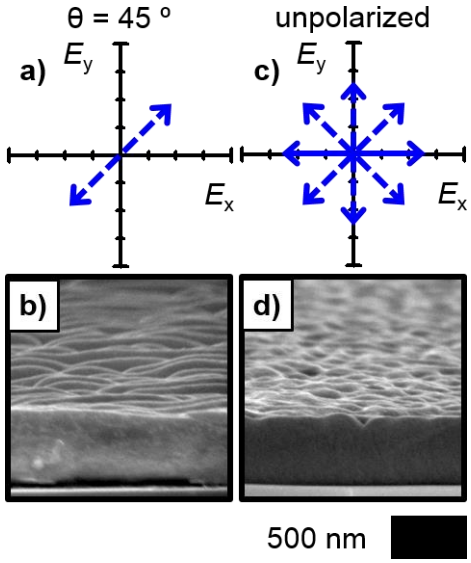

Figure S1. (a) Plot of the E-field vector of a LED source with λ_{avg} = 630 nm linearly polarized 45 **°** clockwise from the vertical, and (b) cross-sectional SEM representative of a photoelectrodeposit generated with this source (cleaved parallel to the long axis of the anisotropic lamellar-type pattern). (c) Plot illustrative of the many E-field vectors characteristic of the same source as in panel a when unpolarized, and (d) cross-sectional SEM representative of a photoelectrodeposit generated with such a source in the unpolarized state.

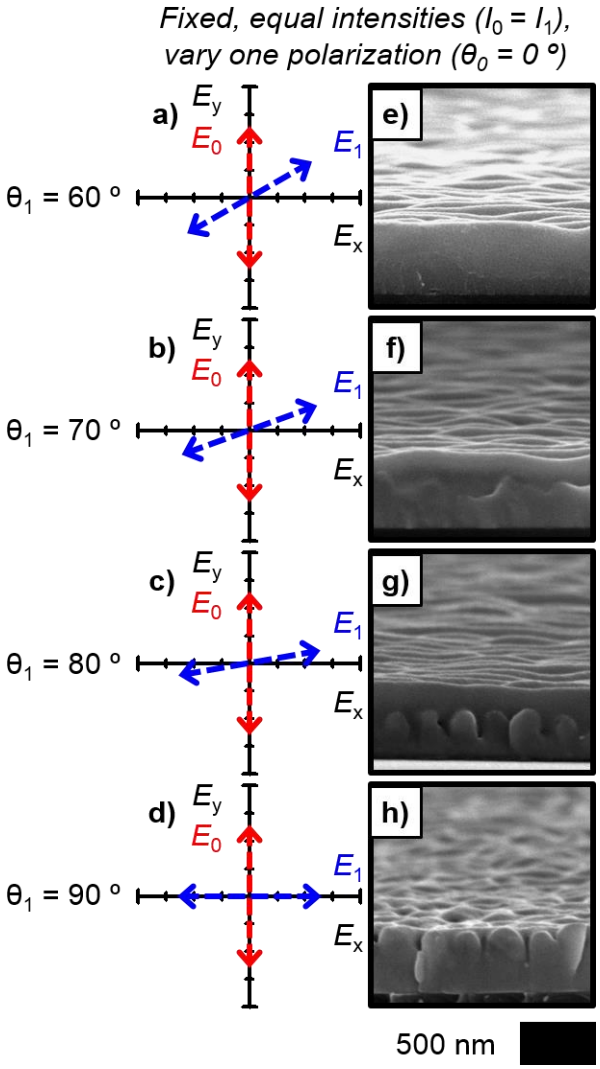

Figure S2. Two-source illumination polarization effect on photoelectrodeposit morphology for near-orthogonal and orthogonal polarizations. (a)-(d) Plots of the E-field vectors, E_0 and E_1, of two incoherent LED sources with λ_{avg} = 630 nm and equal intensity, the first source polarized vertically (θ_0 = 0 °) and the second at the indicated rotation (θ_1) clockwise from the vertical, and (e)-(h) cross-sectional SEMs representative of photoelectrodeposits generated using these sources (cleaved parallel to the long axis of the anisotropic lamellar-type pattern).

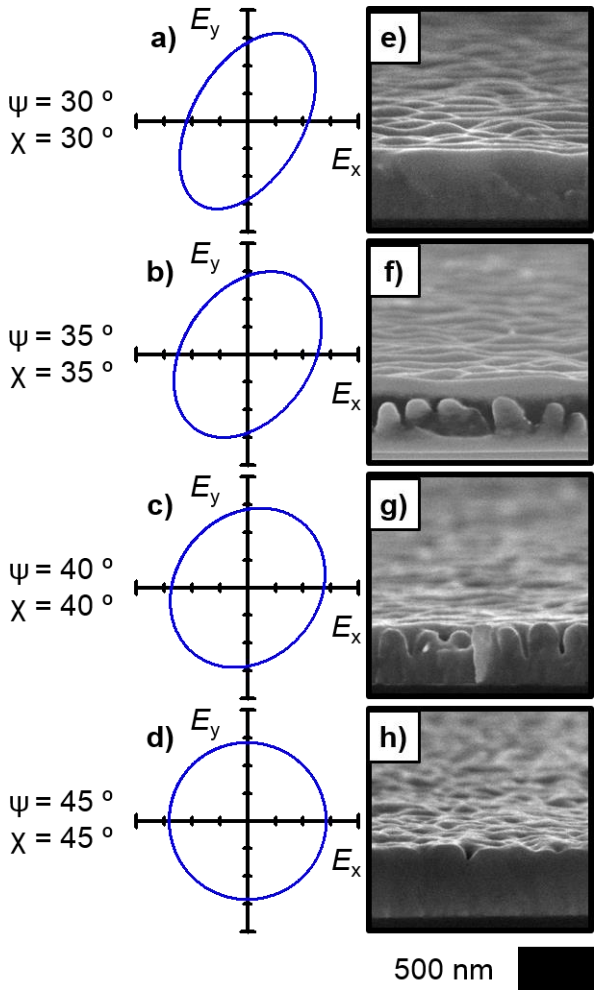

Figure S3. (a)-(d) Plots of the E-field vector traced over time at a fixed point for illumination provided by a HeNe laser λ_{avg} = 632.8 nm with defined elliptical polarizations. ψ indicates the orientation of the major axis of the ellipse measured clockwise from the vertical. χ represents the angle between the major axis and a line connecting a vertex on the major axis with one on the minor axis and relates the eccentricity and asymmetry of the ellipse. (e)-(h) Cross-sectional SEMs representative of photoelectrodeposits generated with the elliptical illumination profiles indicated in panels a-d respectively (cleaved parallel to the long axis of the anisotropic lamellar-type pattern for (e)-(g)).

S5. Elemental Composition Analysis of Photoelectrodeposits

The elemental composition of all of the photoelectrodeposits was analyzed using energy-dispersive X-ray spectroscopy (EDS). All analyzed films were found to be wholly composed of Se and Te. Photoelectrodeposits generated using a single incoherent LED source with λ_{avg} = 633 nm were found to on average have compositions of 56 atomic % Se (remainder Te) both when the illumination was polarized and when the illumination was unpolarized. Figure S4 presents a plot of the elemental composition (in terms of atomic % Se) of the photoelectrodeposits generated by simultaneously using two incoherent LED sources that had λ_{avg} = 630 nm and equal intensities, with the first source polarized vertically ($\theta_0 = 0°$) and the second source offset clockwise from the vertical by θ_1, as a function of θ_1. Figure S5 presents analogous data pertaining to the photoelectrodeposits generated using a HeNe laser with λ_{avg} = 632.8 nm with defined elliptical polarizations wherein $\psi = \chi$, as a function of ψ. In all cases, the average compositions of the photoelectrodeposits were found to range between 53 and 56 atomic % Se.

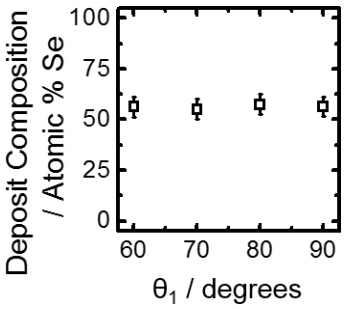

Figure S4. Plot of the elemental composition, in terms of atomic % of Se, of photoelectrodeposits generated using two incoherent LED sources with λ_{avg} = 630 nm and equal intensity, the first source polarized vertically ($\theta_0 = 0$ °) and the second at a defined rotation (θ_1) clockwise from the vertical, as a function of θ_1. Photoelectrodeposits were composed wholly of Se and Te.

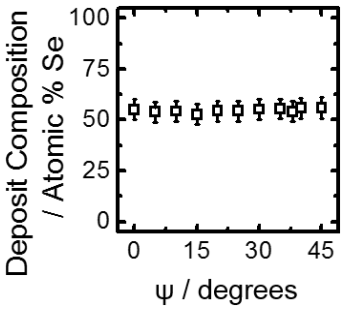

Figure S5. Plot of the elemental composition, in terms of atomic % of Se, of photoelectrodeposits, generated using a HeNe laser with λ_{avg} = 632.8 nm with defined elliptical polarizations wherein $\psi = \chi$, as a function of ψ. ψ indicates the orientation of the major axis of the ellipse measured clockwise from the vertical. χ represents the angle between the major axis and a line connecting a vertex on the major axis with one on the minor axis and relates the eccentricity and asymmetry of the ellipse. Photoelectrodeposits were composed wholly of Se and Te.

S6. Structural Analysis of Photoelectrodeposits

Figure S6 presents a Raman spectrum representative of the Se-Te photoelectrodeposits generated in this work. The spectrum displays modes centered at 96 cm^{-1}, 120 cm^{-1}, 170 cm^{-1}, 201 cm^{-1}, and 240 cm^{-1}. The presence of these modes is consistent with the presence of a substitutional alloy of Se and Te in a hexagonal (trigonal) structure common to both elements in their pure phases.[5]

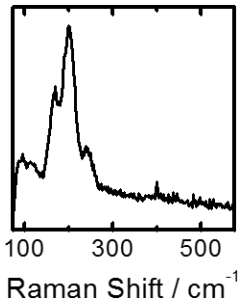

Figure S6. Raman spectrum of a Se-Te photoelectrodeposit generated using an incoherent LED source with λ_{avg} = 630 nm.

S7. References

1. El-Korashy, A.; El-Zahed, H.; Zayed, H. A.; Kenawy, M. A. *Solid State Commun.* **1995**, *95*, 335-339.
2. Mott, N. F.; Davis, E. A., *Electronic Processes in Non-Crystalline Materials*. 2 ed.; Oxford University Press: New York, 1971.
3. Sadtler, B.; Burgos, S. P.; Batara, N. A.; Beardslee, J. A.; Atwater, H. A.; Lewis, N. S. *Proc. Natl. Acad. Sci. U. S. A.* **2013**, *110*, 19707-19712.
4. Hale, G. M.; Querry, M. R. *Appl. Opt.* **1973**, *12*, 555-563.
5. Geick, R.; Steigmeier, E. F.; Auderset, H. *Phys. Status Solidi B* **1972**, *54*, 623-630.